ACS APPLIED MATERIALS & INTERFACES

Research Article

www.acsami.org

Selective Modification of Halloysite Nanotubes with 1-Pyrenylboronic Acid: A Novel Fluorescence Probe with Highly Selective and Sensitive Response to Hyperoxide

Hailei Zhang, Tianfei Ren, Yunjing Ji, Lingui Han, Yonggang Wu,* Hongzan Song,* Libin Bai, and Xinwu Ba

College of Chemistry and Environmental Science, Hebei University, Baoding 071002, China

Supporting Information

ABSTRACT: A novel fluorescence probe based on modified halloysite nanotubes (HNTs) by using 1-pyrenylboronic acid selectively grafted onto the inner surface of lumen was successfully achieved. The solid-state nuclear magnetic resonance (^{13}C and ^{11}B), X-ray photoelectron spectroscopy (XPS) and Fourier transform infrared (FTIR) confirmed that the boronic acid group only binds to alumina at the tube lumen and does not bind the tube's outer siloxane surface. The modified HNTs (HNTs-PY) inherit the spectroscopic properties relating to the pyrene units. Interestingly, the established Al−O−B linkage gives the H_2O_2-sensitivity to pyrene grafted tubes. HNTs-PY exhibits a highly specific "turn-off" response for hyperoxide over other reactive oxygen species (ROS) and oxidative ions owing to their chemoselective boronate-to-phenol switch. The "turn-off" response can even be tracked when the additional amount of H_2O_2 was limited to 1×10^{-6} mol. Thus, the selective modification method under mild conditions for the design of novel organic−inorganic hybrid fluorescence probe may open up a broader application as well as for identification and diagnosis.

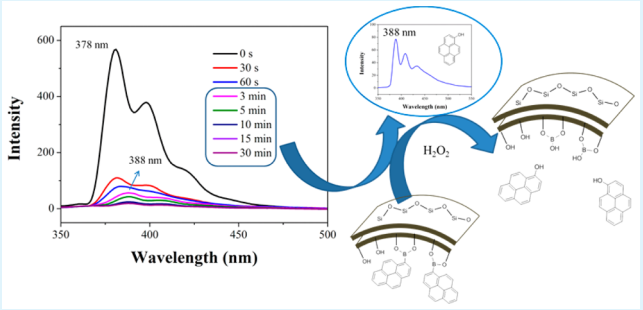

KEYWORDS: *halloysite nanotubes, selective modification, fluorescence probe, hyperoxide, 1-pyrenylboronic acid*

1. INTRODUCTION

Halloysite nanotubes (HNTs) have garnered interest in material science due to their versatile advantages of biocompatibility, environmental friendliness, large surface area, and high porosity, as well as low cost and widely spreadable properties.[1−3] HNTs ($Al_2Si_2O_5(OH)_4 \cdot nH_2O$) are hollow like aluminosilicate clay, similar to commonly used platy clay kaolin.[4−6] The size of HNTs often ranges from 15 to 100 nm in external diameter with a length from 500 to 1000 nm. Neighboring alumina and silica layers, accompanying their hydration effect with water, lead to a packing disorder causing sheets to curve and roll up, forming multilayer nanotubes.[7] Generally, the internal surface of HNTs consists of a gibbsite octahedral array (Al−OH) groups, whereas the siloxane groups (Si−O−Si) overspread on the external surface. Usually, the inner and outer-compositions of these tubes allow for quite a few feasible modification methods by immobilization of functional groups via different chemical reactions, which can open up some attractive applications including including catalysis,[8−10] anticorrosion,[11,12] adsorbent,[13,14] drug delivery,[15−19] enzyme immobilization,[20] aerogel,[21] rubber filler,[22] fiber spinning,[23,24] and electronic devices.[25−27] However, some classical methods often result in the nonspecific modification of both inner and outer surfaces.[28] The modification of the halloysite tube outer surface is usually intended to decrease the clay dispersal in aqueous media. Therefore, selective modification with functional molecules for inner surface offers great promise for hybrid HNT-based materials,[14,29,30] which, however, remains a difficult task.

A potential new tool for selective modification of silica-alumininm oxides materials is arylboronic acid. Early studies of alcohol-affinitive molecules revealed that arylboronic acid can rapidly react with diols in mild conditions; the reaction between arylboronic acid and pinacol is one of the most typical cases in organic chemistry. Moreover, the diboronic acid can be easily developed as an interlinker aiming to developing graphene oxide nanoporous materials with better gas adsorption properties.[31,32] Therefore, we demonstrate here that the arlyboronic acid can also be covalently linked to the alumina innermost surface but not to the silica outermost surface of HNTs. Following this way, the plane-conjugated molecules can be immobilized onto the lumen surface to functionalize the modified HNTs with fluorescence properties.

In the past decades, organic−inorganic hybrid fluorescence probes, especially nanoparticle-based fluorescence probes, played a crucial role in modern analysis fields.[33−35] It is also full of meaningness to develop tubular hybrid materials which

Received: September 12, 2015
Accepted: October 9, 2015
Published: October 9, 2015

DOI: 10.1021/acsami.5b08600
ACS Appl. Mater. Interfaces 2015, 7, 23805−23811

Scheme 1. Selective Modification of the Alumina Innermost Surface

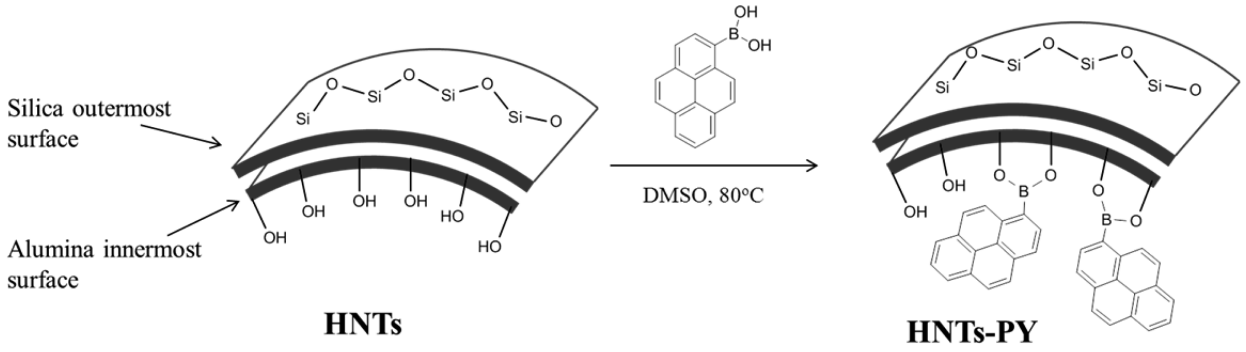

can be used as fluorescence probes. Interestingly, recent investigations clearly showed that the deprotection of aryl boronates to phenols provided a reaction-based approach to specific fluorescence detection of hydrogen peroxide (H_2O_2).[36−39] H_2O_2 is viewed as a marker for oxidative stress and damage events in vivo. Recent investigations also suggest that H_2O_2 serve as a newly recognized messenger in cellular signal transduction.[40,41] Developing new chemical tools that are sensitive enough to report H_2O_2 production at low levels while maintaining H_2O_2 specificity over similar reactive oxygenspecies (ROS) is the key to understanding the role H_2O_2 plays in intracellular signaling transduction, normal cell function and cell damage.[42−45] Herein, we hope that the obtained tubular hybrid material is sensitive enough to detect H_2O_2 at a low levels and specific over other ROS owing to their chemoselective boronate switch.

2. EXPERIMENTAL SECTION

2.1. Materials and Methods. HNTs were obtained from GuangZhouShinshi Metallurgy and Chemical Company Ltd. (Guangzhou, China). 1-Pyrenylboronic acid (PBA) was purchased from Sigma-Aldrich. Aluminum oxide nanometer (30 nm) and silica nanospheres (50 nm) were purchased from J&K Chemical Technology. Sodium nitroferricyanide ($Na_2Fe(CN)_5NO$), *t*-butylhydroperoxide (TBHP), and sodium hypochlorite (NaClO) were purchased from Aladdin Industrial Incorporated. Dimethyl sulfoxide (DMSO) was dried and distilled from CaH_2 under vacuum before use. Distilled water was used throughout the study. High-purity argon was used for degassing procedures.

2.2. Preparation. *2.2.1. Purification of HNTs.* HNTs were purified according to our previous work.[46]

2.2.2. Preparation of HNTs-PY. A mixture of purified HNTs (200 mg) and PBA (400 mg) in anhydrous DMSO was carefully degassed. The system was heated at 80 °C for 6 h under stirring. The mixture was cooled to ambient temperature and then washed triply and sequentially by ethyl acetate, methanol, and dichloromethane. The residue was collected by centrifugation. After vacuum-drying, the HNTs-PY was obtained as a faint yellow solid.

2.2.3. Preparation of H_2O_2-Treated HNTs-PY. A suspension of H_2O_2 (5 mmol) and HNTs (50 mg) in 10 mL of water was mixed in a flask under magnetic stirring at room temperature for 10 min. The tubes were washed triply and sequentially by ethyl acetate, methanol and dichloromethane. The residue was vacuum-dried to give H_2O_2 treated HNTs-PY as a faint yellow solid.

2.2.4. Generation of reactive oxygen species (ROS). Nitric oxide (NO•) was generated from sodium nitroferricyanide ($Na_2Fe(CN)_5NO$).[47] H_2O_2, TBHP, and ClO^- were delivered from 30% H_2O_2, 70% TBHP, and 5% NaClO aqueous solutions, respectively.

2.2.5. Characterizations. UV−visible absorption spectra were obtained on a Shimadzu UV−visible spectrometer model UV-2550. Fluorescence spectra were recorded on a Shimadzu RF-5301PC. TGA was performed on PerkinElmer Pyris 6 under a nitrogen flow. Accurately weighted amounts of samples were heated at a scanning rate of 10 °C/min from 40 to 800 °C. The morphological characterizations were performed by using a Tecnai G2 F20 S-TWIN transmission electron microscope (TEM) with an accelerating voltage of 200 kV. FTIR spectra were recorded in the region of 400−4000 cm^{-1} for each sample on a Varian-640 spectrophotometer. Samples were previously grounded and mixed thoroughly with KBr. The spectrum for each sample was obtained from averaging 32 scans over the selected wavenumber range. Solid-state NMR (^{13}C and ^{11}B) spectra were obtained on a Bruker Advance III spectrometer. X-ray photoelectron spectroscopy (XPS) was carried out on a Thermo Scientific ESCALab 250Xi using 200 W monochromated Al Kα radiation. The 500 μm X-ray spot was used for XPS analysis. The base pressure in the analysis chamber was about 3×10^{-10} mbar. Typically the hydrocarbon C 1s line at 284.8 eV from adventitious carbon was used for energy referencing.

3. RESULTS AND DISCUSSION

3.1. Synthesis and Structural Characterizations. In this study, purified HNTs were treated with an excess of PBA to couple boric acid with hydroxyl groups over the alumina innermost surface via a solvothermal method (Scheme 1). DMSO was used as reaction solvent to satisfy both the solubility of PBA and dispersibility of the nanotubes. HNTs exhibited better dispersibility in DMSO than in other organic solvents including *N*,*N*-dimethylformamide, tetrahydrofuran, methanol, ethyl acetate, dichloromethane, and chloroform. The use level was limited to a minimal amount aiming to favor a desirable grafting efficiency. Unreacted compounds were removed by thorough washing with good solvents including ethyl acetate, methanol and dichloromethane.

The differences in the composition of nanotube samples were revealed by the solid-state NMR (^{13}C and ^{11}B) spectra and XPS analysis. The solid-state ^{13}C NMR spectra of HNTs, HNTs-PY, and PBA are depicted in Figure 1. The spectrum of PBA displays sharp resonances in the region from 135 to 110 ppm for all 16 carbon environments of the molecule. The ^{13}C NMR spectra indicate that the chemical environment of HNTs-PY is somewhat different from the original HNTs of which spectrum shows no obvious signals in the region from 250 to 100 ppm. The weak resonance peaked at 122.3 ppm in the spectrum of HNTs-PY is corresponding to pyrene groups. The solid-state ^{11}B NMR spectrum of HNTs, shown in Figure S1, reveals that little boron exists in original halloysite. Whereas HNTs-PY displays weak peaks centralizing at 15.1 and 0.1 ppm, indicating the presence of the boron in modified HNTs. The upfield shifts suggest that the chemical environment of boron in HNTs-PY is different from that in PBA.

The XPS spectra (Figure 2) of original HNTs and modified HNTs show the presence of aluminum (Al 2s and Al 2p) and silicon (Si 3p), in accordance with the composition of alumino-

DOI: 10.1021/acsami.5b08600
ACS Appl. Mater. Interfaces 2015, 7, 23805−23811

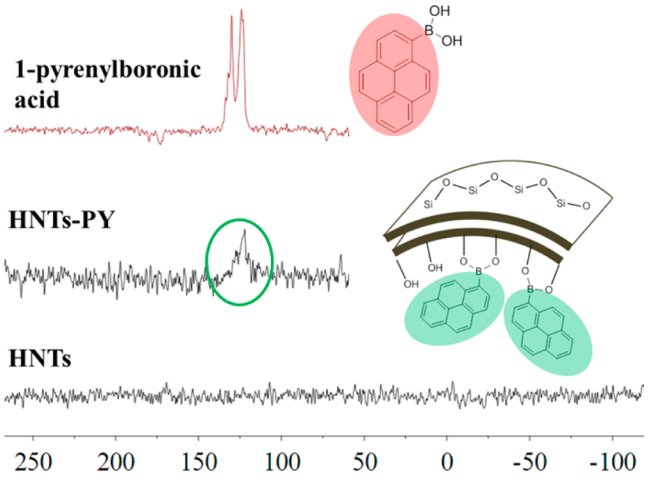

Figure 1. Solid-state ^{13}C NMR spectra of HNTs, HNTs-PY, and PBA.

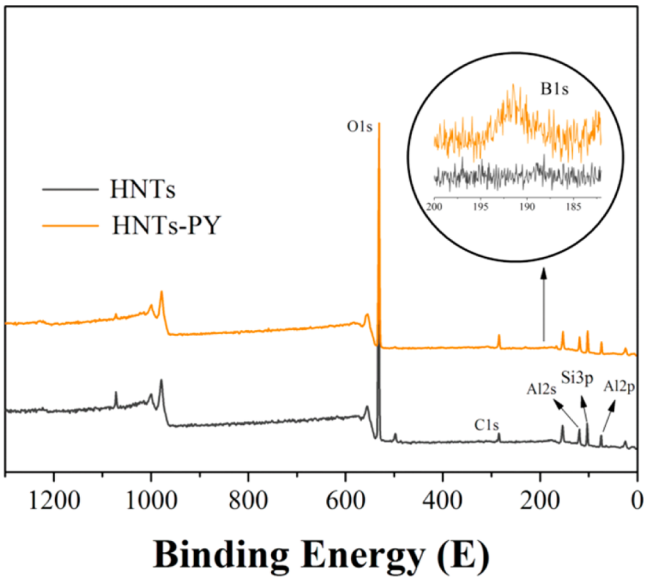

Figure 2. XPS spectra of original HNTs and HNTs-PY.

silicate clay. The weak signal in the curve of original HNTs suggests that some organic component exists in the multilayer nanotubes. As for HNTs-PY, areas relating to C 1s appeared to be slightly larger suggesting some organic contents have be grafted. It should be noted that the weak peak assigned to B 1s can be tracked at 191.5 eV. Generally, the wall thickness of HNTs exceeds the penetration depth of XPS (10 nm).[29] So it is difficult to disclose the chemical composition of the inner lumen surface. The weak change in the spectrum of HNTs-PY may be attributed to the fractions grafted on the opening of the tubes, which are partially exposed to X-rays.

The FTIR spectra of original HNTs and modified HNTs are depicted in Figure 3. Original HNTs feature two distinct peaks at 3703 and 3625 cm^{-1}. Inner hydroxyl groups, lying between the tetrahedral and octahedral sheets, give the absorption near 3625 cm^{-1}. The other strong band at 3703 cm^{-1} is related to the surface hydroxyl groups in the lumen of the nanotubes.[48] Characteristic band of in-plane Si−O−Si stretching vibration can be observed around 1036 cm^{-1}. The bands less than 1000 cm^{-1} can be assigned to symmetric or perpendicular stretching vibrations of Si−O or Al−O groups. As for HNTs-PY, the distinct band corresponding to surface hydroxyl groups in the

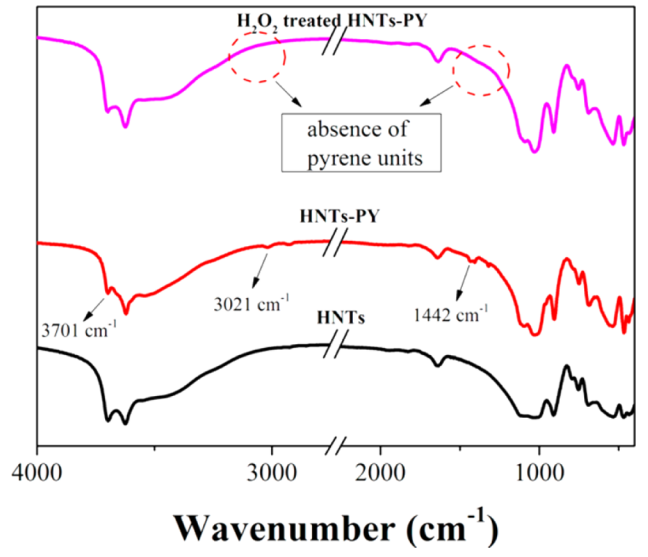

Figure 3. FTIR spectra of original HNTs, HNTs-PY, and H_2O_2-treated HNTs-PY.

lumen at 3701 cm^{-1} displays an obvious decrease, suggesting the consumption of surface hydroxyl groups in lumen during the grafting reaction. Moreover, the grafting of pyrene onto the nanotube is confirmed from the characteristic C−H stretching and benzene skeleton vibrations centered at 3035 and 1442 cm^{-1}, respectively. The quantity of the pyrene grafted to the nanotube was calculated to be 6.2 wt % by thermogravimetric analysis (TGA, Figure 4). Otherwise, the products with higher

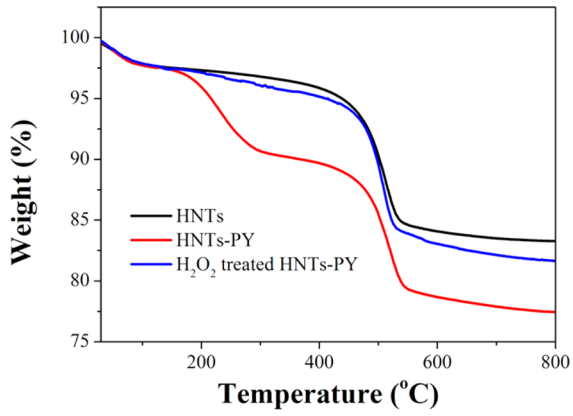

Figure 4. TGA curves of original HNTs, HNTs-PY, and H_2O_2-treated HNTs-PY.

grafting degrees can be achieved by extending the reaction time. For an example, the modified HNTs prepared by treating HNTs with PBA for 48 h possess a grafting degree of 12.2% (the thermogravimetric analysis was shown in Figure S2); in addition, the FT-IR spectrum of the modified HNTs by treating HNTs with PBA for 48 h depicted in Figure S3 shows stronger benzene skeleton vibrations and a disappearance of the peak assigned to surface hydroxyl groups in the lumen.

3.2. Investigation of Selective Modification Nature. Halloysite nanotube is a dioctahedral 1:1 layered aluminosilicate. The outermost surface is made of a silica-type layer in which the oxygen atoms are tetrahedrally coordinated by silicon atoms. The innermost Gibbsite-type layer makes the lumen shows hydroxyl groups. Therefore, we hypothesized that grafting reaction should

DOI: 10.1021/acsami.5b08600
ACS Appl. Mater. Interfaces 2015, 7, 23805−23811

be a selective modification of halloysite lumen. Then, a model experiment conducted by Takahara et al. was employed in this study to verify this point.[30] In the model experiment, Al_2O_3 nanoparticles were also treated with PBA in DMSO at 80 °C for 6 h.Then the particles were washed triply and sequentially by ethyl acetate, methanol and dichloromethane. For PBA-treated Al_2O_3 particles, the FTIR spectrum shown in Figure S4A displays a new strong band located at 1437 cm^{-1} and a weak stretching centralizing at 3034 cm^{-1}, which can be attributed to the grafted pyrene units. However, when SiO_2 nanoparticles were treated with PBA in same conditions, pyrene units cannot be tracked in the FTIR spectrum of PBA-treated SiO_2 nanoparticles (Figure S4B). The result is also applicable to the alumina and silica surfaces of halloysite.

3.3. Morphological Characterizations. TEM images of original HNTs and modified HNTs are shown in Figure 5. Figure

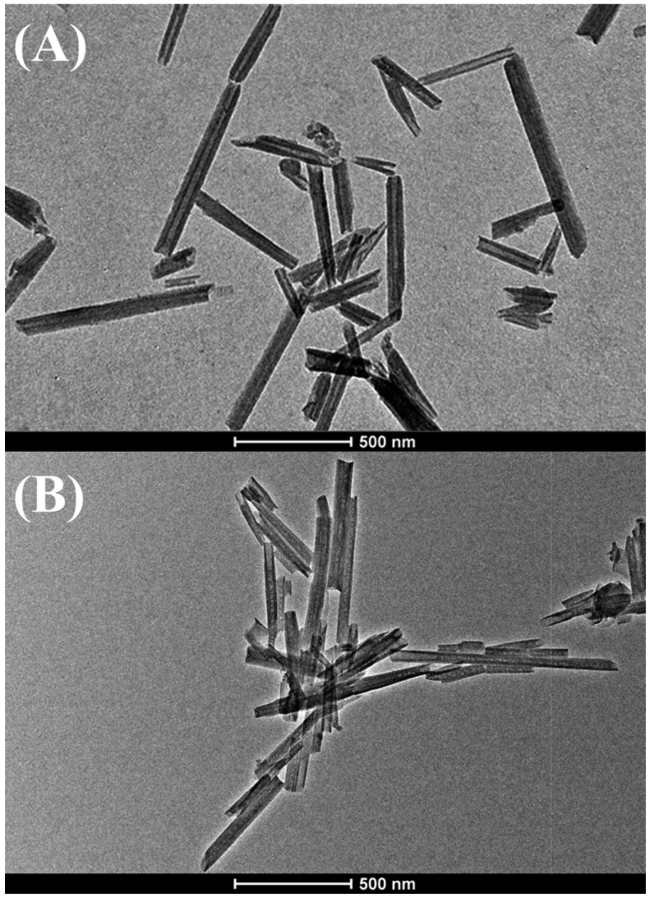

Figure 5. TEM images of (A) HNTs and (B) HNTs-PY.

5A reveals that the original HNTs are cylindrical shaped with an open-ended lumen along the nanotubes. The nanotubes have an outer diameter of 40−60 nm and a lumen diameter of 15−25 nm, while the wall thickness is about 20 nm. After modification, the nanotubes possess similar overall morphologies to those of original HNTs, indicating the nanotube underwent little damage during the modification procedure. Moreover, the transparent central channel becomes less resolved at a higher resolution. As seen in Figure 5B, the lumen is almost completely filled. Otherwise, the tubes after modification retained the smooth outmost surface. Therefore, it can be also inferred from the TEM micrographs that the pyrene units were selectively grafted in the lumen of HNTs, which can be served as a direct proof to verify the selective modification and grafting procedures.

3.4. Spectroscopic Properties and Responses to Hydrogen Peroxide. The absorption spectra of original HNTs and HNTs-PY were measured in aqueous solution, as shown in Figure S6. The original HNTs display almost no absorption peaks in the region from 300 to 600 nm. After modification, HNTs-PY features two weak absorption peaks around 323 and 340 nm which can be attributed to the introduction of pyrene units. Photoluminescence behaviors were also investigated in aqueous solution. When excited at 300 nm, the original HNTs exhibited no fluorescence properties. HNTs-PY displays a strong emission peak at 380 nm. The quantum yield (Φ_f) of HNTs-PY was calculated as 0.63, with quinine sulfate (Φ_f = 0.55 in 0.05 M H_2SO_4) as the reference standard.

The addition of H_2O_2 into HNTs-PY aqueous dispersion triggered a marked decrease in fluorescence intensity. The treated suspension displays a weak emission peak at 388 nm, which is corresponding to the emission spectrum of 1-hydroxypyrene; there is a bathochromic shift of 8 nm relative to the emission peak of HNTs-PY. Otherwise, the escape of the pyrene units from nanotubes can be tracked in the FT-IR spectrum of H_2O_2-treated HNTs-PY. The weight loss can be confirmed by TGA curve of H_2O_2 treated HNTs-PY. The response mechanism is summarized in Scheme 2. When PBA immobilized on to the alumina innermost surface, the nanotubes with pyrene groups can also retain the desirable dispersibility in aqueous media and possess attractive fluorescence property emitting centralizing at 380 nm. The aromatic boronic acid derivatives can transform into 1-hydroxypyrene in a few minutes in the presence of excess amount of H_2O_2. The poor water solubility of 1-hydroxypyrene result in a dramatically decrease of the fluorescence intensity. Yet, some generated 1-hydroxypyrene in the initial stage of the generation may be loaded in the lumen of the tubes, which retained some water-soluble property in accompany with the hydrophilic halloysite. As time goes on, these loaded compounds also escaped from the lumen following a sustained-release manner result in the mild decrease at the last stage.

The sensitivity of HNTs-PY to H_2O_2 was also investigated by fluorescence spectroscopy. Upon addition of H_2O_2 at different amount into the HNTs-PY aqueous suspension, the reduction of the fluorescence intensity even can be tracked when the addition amount of H_2O_2 decreasing to 1×10^{-6} mol (Figure S7). Otherwise, the sensitivity of modified nanotubes (HNTs-PY2) with higher grafting ratio (12.2%) was also investigated. The response behaviors of HNTs-PY2 did not display significant difference from 1×10^{-3} to 1×10^{-7} mol H_2O_2 (Figure S8) when compared to those of HNTs-PY, suggesting that the performance of as-prepared fluorescent probe presented little relationships to the ratio of fluorescent molecules grafted on the nanotubes. Owing to their chemoselective boronate switch, HNTs-PY retains highly specific responses to H_2O_2. Other groups did not show relative turn-off fluorescence when treating with ROS agents including NO• and ClO^- (Figure 6). Moreover, the fluorescence intensity of HNTs-PY was found to be almost unaffected by the addition of Fe^{3+}, Cu^{2+}, Cr^{3+}, $H_2PO_4^-$, SO_4^{2-}, $S_2O_3^{2-}$, and NO_3^- (Figure S9). The result indicates that the turn-off fluorescence can also be tracked in term of lipid peroxide, such as *t*-butylhydroperoxide (TBHP). Therefore, HNTs-PY exhibits excellent selectivity toward hyperoxides.

DOI: 10.1021/acsami.5b08600
ACS Appl. Mater. Interfaces 2015, 7, 23805−23811

Scheme 2. Response Mechanism of HNTs-PY to Hydrogen Peroxide and the Fluorescence Spectra of HNTs-PY Aqueous Suspension ([*c*] = 0.1 mg/mL) after Addition of H_2O_2 (1×10^{-3} mol)[a]

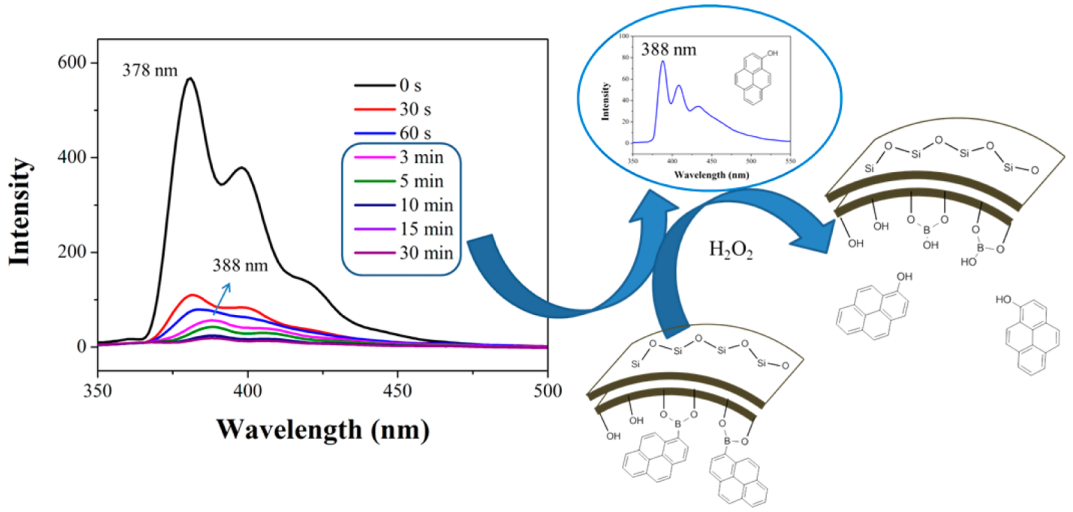

[a]Conditions: excitation wavelength, 300 nm; 2 mL of HNTs-PY aqueous suspension was used.

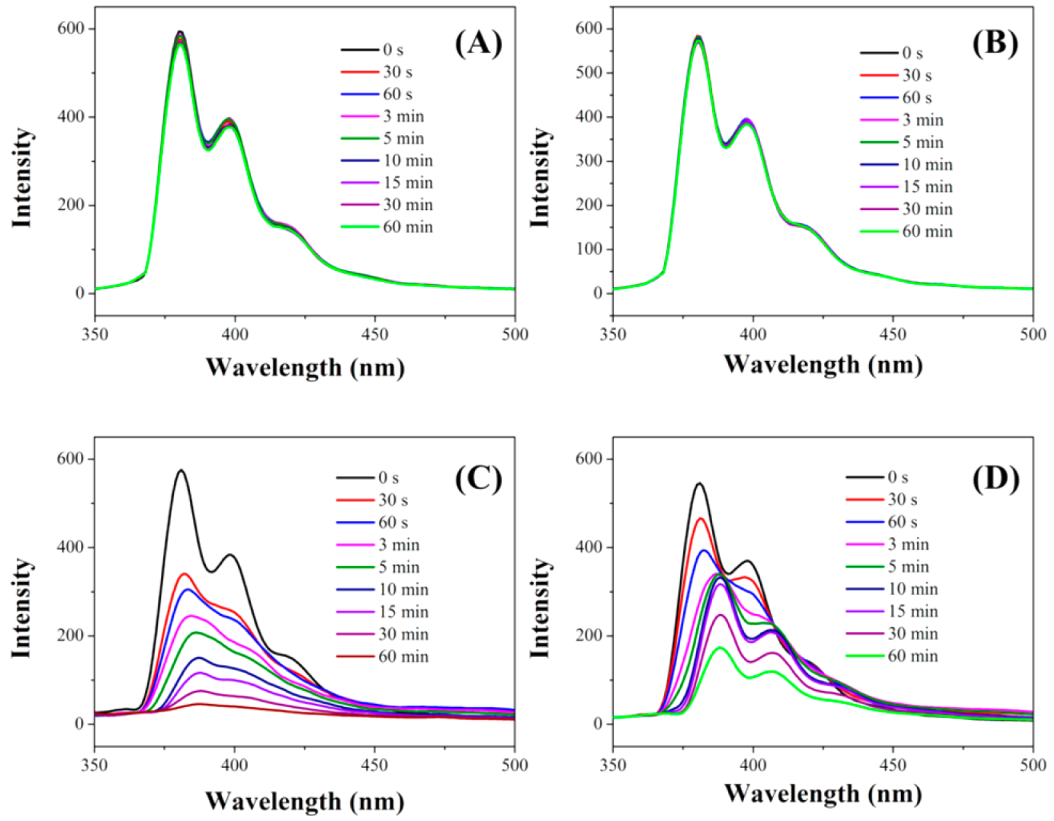

Figure 6. Fluorescence spectra of HNTs-PY aqueous suspension ([*c*] = 0.1 mg/mL) after addition of ClO^- (A, 1×10^{-4} mol), NO· (B, 1×10^{-4} mol), H_2O_2 (C, 1×10^{-4} mol) and TBHP (D, 1×10^{-4} mol). Conditions: excitation wavelength, 300 nm; 2 mL of HNTs-PY aqueous suspension was used for each test.

4. CONCLUSIONS

In this work, we developed an efficient method to functionalize the HNTs with pyrene units. PBA was found to bind to alumina sites at the tube lumen and did not bind the tube's outer siloxane surface. The final nanocomposite retained regular morphology and desirable dispersibility in aqueous solution. The established Al−O−B linkage gives a highly specific and sensitive H_2O_2-sensitivity to HNTs-PY, as a result the fluorescence exhibits a highly specific "turn-off" response for hyperoxide. The selective modification method explored in this study can be also appropriate for other arylboronic acid derivatives, which may create more applications of HNTs. Further investigations should be conducted to verify whether the Al−O−B linkage established by other compounds can also exhibit a highly specific and sensitive response to hyperoxide.

DOI: 10.1021/acsami.5b08600
ACS Appl. Mater. Interfaces 2015, 7, 23805−23811

■ ASSOCIATED CONTENT

Supporting Information

The Supporting Information is available free of charge on the ACS Publications website at DOI: 10.1021/acsami.5b08600.

Solid-state ^{11}B NMR spectra, TGA curve and FT-IR spectrum of HNT-PY2, FT-IR spectra of PBA treated Al_2O_3 and SiO_2 nanoparticles, detailed TEM images, UV−vis absorption spectra andthe fluorescence spectra for sensitive and selective studies (PDF)

■ AUTHOR INFORMATION

Corresponding Authors

*E-mail: wuyonggang@hbu.edu.cn.
*E-mail: songhongzan@iccas.ac.cn.

Notes

The authors declare no competing financial interest.

■ ACKNOWLEDGMENTS

This work was supported by the National Science Foundation of China (Grant Nos. 21274037, 21304029, and 21474026).

■ REFERENCES

(1) Liu, M.; Jia, Z.; Jia, D.; Zhou, C. Recent Advance in Research on Halloysite Nanotubes-Polymer Nanocomposite. *Prog. Polym. Sci.* **2014**, *39*, 1498−1525.

(2) Lvov, Y.; Abdullayev, E. Functional Polymer-Clay Nanotube Composites with Sustained Release of Chemical Agents. *Prog. Polym. Sci.* **2013**, *38*, 1690−1719.

(3) Lvov, Y.; Aerov, A.; Fakhrullin, R. Clay Nanotube Encapsulation for Functional Biocomposites. *Adv. Colloid Interface Sci.* **2014**, *207*, 189−198.

(4) Cavallaro, G.; Lazzara, G.; Milioto, S. Exploiting the Colloidal Stability and Solubilization Ability of Clay Nanotubes/Ionic Surfactant Hybrid Nanomaterials. *J. Phys. Chem. C* **2012**, *116*, 21932−21938.

(5) Cavallaro, G.; Lazzara, G.; Milioto, S. Dispersions of Nanoclays of Different Shapes into Aqueous and Solid Biopolymeric Matrices. Extended Physicochemical Study. *Langmuir* **2011**, *27*, 1158−1167.

(6) Guimaraes, L.; Enyashin, A. N.; Seifert, G.; Duarte, H. A. Structural, Electronic, and Mechanical Properties of Single-Walled Halloysite Nanotube Models. *J. Phys. Chem. C* **2010**, *114*, 11358−11363.

(7) Lvov, Y. M.; Shchukin, D. G.; Mohwald, H.; Price, R. R. Halloysite Clay Nanotubes for Controlled Release of Protective Agents. *ACS Nano* **2008**, *2*, 814−820.

(8) Abdullayev, E.; Sakakibara, K.; Okamoto, K.; Wei, W. B.; Ariga, K.; Lvov, Y. Natural Tubule Clay Template Synthesis of Silver Nanorods for Antibacterial Composite Coating. *ACS Appl. Mater. Interfaces* **2011**, *3*, 4040−4046.

(9) Sanchez-Ballester, N. M.; Ramesh, G. V.; Tanabe, T.; Koudelkova, E.; Liu, J.; Shrestha, L. K.; Lvov, Y.; Hill, J. P.; Ariga, K.; Abe, H. Activated Interiors of Clay Nanotubes for Agglomeration-Tolerant Automotive Exhaust Remediation. *J. Mater. Chem. A* **2015**, *3*, 6614−6619.

(10) Wang, R.; Jiang, G.; Ding, Y.; Wang, Y.; Sun, X.; Wang, X.; Chen, W. Photocatalytic Activity of Heterostructures Based on TiO_2 and Halloysite Nanotubes. *ACS Appl. Mater. Interfaces* **2011**, *3*, 4154−4158.

(11) Abdullayev, E.; Price, R.; Shchukin, D.; Lvov, Y. Halloysite Tubes as Nanocontainers for Anticorrosion Coating with Benzotriazole. *ACS Appl. Mater. Interfaces* **2009**, *1*, 1437−1443.

(12) Abdullayev, E.; Abbasov, V.; Tursunbayeva, A.; Portnov, V.; Ibrahimov, H.; Mukhtarova, G.; Lvov, Y. Self-Healing Coatings Based on Halloysite Clay Polymer Composites for Protection of Copper Alloys. *ACS Appl. Mater. Interfaces* **2013**, *5*, 4464−4471.

(13) Liu, Y.; Jiang, X.; Li, B.; Zhang, X.; Liu, T.; Yan, X.; Ding, J.; Cai, Q.; Zhang, J. Halloysite Nanotubes@Reduced Graphene Oxide Composite for Removal of Dyes from Water and as Supercapacitors. *J. Mater. Chem. A* **2014**, *2*, 4264−4269.

(14) Cavallaro, G.; Lazzara, G.; Milioto, S.; Parisi, F.; Sanzillo, V. Modified Halloysite Nanotubes: Nanoarchitectures for Enhancing the Capture of Oils from Vapor and Liquid Phases. *ACS Appl. Mater. Interfaces* **2014**, *6*, 606−612.

(15) Massaro, M.; Riela, S.; Lo Meo, P.; Noto, R.; Cavallaro, G.; Milioto, S.; Lazzara, G. Functionalized Halloysite Multivalent Glycocluster as A New Drug Delivery System. *J. Mater. Chem. B* **2014**, *2*, 7732−7738.

(16) Abdullayev, E.; Lvov, Y. Halloysite Clay Nanotubes as A Ceramic "Skeleton" for Functional Biopolymer Composites with Sustained Drug Release. *J. Mater. Chem. B* **2013**, *1*, 2894−2903.

(17) Riela, S.; Massaro, M.; Colletti, C. G.; Bommarito, A.; Giordano, C.; Milioto, S.; Noto, R.; Poma, P.; Lazzara, G. Development and Characterization of Co-Loaded Curcumin/Triazole-Halloysite Systems and Evaluation of Their Potential Anticancer Activity. *Int. J. Pharm.* **2014**, *475*, 613−623.

(18) Fan, L.; Zhang, J.; Wang, A. In Situ Generation of Sodium Alginate/Hydroxyapatite/Halloysite Nanotubes Nanocomposite Hydrogel Beads as Drug-Controlled Release Matrices. *J. Mater. Chem. B* **2013**, *1*, 6261−6270.

(19) Liu, M.; Wu, C.; Jiao, Y.; Xiong, S.; Zhou, C. Chitosan-Halloysite Nanotubes Nanocomposite Scaffolds for Tissue Engineering. *J. Mater. Chem. B* **2013**, *1*, 2078−2089.

(20) Chao, C.; Liu, J.; Wang, J.; Zhang, Y.; Zhang, B.; Zhang, Y.; Xiang, X.; Chen, R. Surface Modification of Halloysite Nanotubes with Dopamine for Enzyme Immobilization. *ACS Appl. Mater. Interfaces* **2013**, *5*, 10559−10564.

(21) Chen, H. B.; Wang, Y. Z.; Schiraldi, D. A. Preparation and Flammability of Poly(vinyl alcohol) Composite Aerogels. *ACS Appl. Mater. Interfaces* **2014**, *6*, 6790−6796.

(22) Fu, Y.; Zhao, D.; Yao, P.; Wang, W.; Zhang, L.; Lvov, Y. Highly Aging-Resistant Elastomers Doped with Antioxidant-Loaded Clay Nanotubes. *ACS Appl. Mater. Interfaces* **2015**, *7*, 8156−8165.

(23) Luo, Z.; Wang, A.; Wang, C.; Qin, W.; Zhao, N.; Song, H.; Gao, J. Liquid Crystalline Phase Behavior and Fiber Spinning of Cellulose/Ionic Liquid/Halloysite Nanotubes Dispersions. *J. Mater. Chem. A* **2014**, *2*, 7327−7336.

(24) Tao, D.; Higaki, Y.; Ma, W.; Wu, H.; Shinohara, T.; Yano, T.; Takahara, A. Chain Orientation in Poly(glycolic acid)/Halloysite Nanotube Hybrid Electrospun Fibers. *Polymer* **2015**, *60*, 284−291.

(25) Wan, C. Y.; Li, M.; Bai, X.; Zhang, Y. Synthesis and Characterization of Photoluminescent Eu(III) Coordination Halloysite Nanotube-Based Nanohybrids. *J. Phys. Chem. C* **2009**, *113*, 16238−16246.

(26) Liang, J.; Fan, Z.; Chen, S.; Ding, S.; Yang, G. Hierarchical $NiCo_2O_4$ Nanosheets@halloysite Nanotubes with Ultrahigh Capacitance and Long Cycle Stability As Electrochemical Pseudocapacitor Materials. *Chem. Mater.* **2014**, *26*, 4354−4360.

(27) Liang, J.; Dong, B.; Ding, S.; Li, C.; Li, B. Q.; Li, J.; Yang, G. Facile Construction of Ultrathin Standing Alpha-$Ni(OH)_2$ Nanosheets on Halloysite Nanotubes and Their Enhanced Electrochemical Capacitance. *J. Mater. Chem. A* **2014**, *2*, 11299−11304.

(28) Zhang, H.; Zhu, X.; Wu, Y.; Song, H.; Ba, X. High-efficiency Grafting of Halloysite Nanotubes by Using π-Conjugated Polyfluorenes via "Click" Chemistry. *J. Mater. Sci.* **2015**, *50*, 4387−4395.

(29) Yah, W. O.; Takahara, A.; Lvov, Y. M. Selective Modification of Halloysite Lumen with Octadecylphosphonic Acid: New Inorganic Tubular Micelle. *J. Am. Chem. Soc.* **2012**, *134*, 1853−1859.

(30) Yah, W. O.; Xu, H.; Soejima, H.; Ma, W.; Lvov, Y. M.; Takahara, A. Biomimetic Dopamine Derivative for Selective Polymer Modification of Halloysite Nanotube Lumen. *J. Am. Chem. Soc.* **2012**, *134*, 12134−12137.

(31) Srinivas, G.; Burress, J. W.; Ford, J.; Yildirim, T. Porous Graphene Oxide Frameworks: Synthesis and Gas Sorption Properties. *J. Mater. Chem.* **2011**, *21*, 11323−11329.

(32) Burress, J. W.; Gadipelli, S.; Ford, J.; Simmons, J. M.; Zhou, W.; Yildirim, T. Graphene Oxide Framework Materials: Theoretical Predictions and Experimental Results *Angew. Angew. Chem., Int. Ed.* **2010**, *49*, 8902−8904.

DOI: 10.1021/acsami.5b08600
ACS Appl. Mater. Interfaces 2015, 7, 23805−23811

(33) Zhang, X.; Zhang, X.; Wang, S.; Liu, M.; Zhang, Y.; Tao, L.; Wei, Y. Facile Incorporation of Aggregation-Induced Emission Materials into Mesoporous Silica Nanoparticles for Intracellular Imaging and Cancer Therapy. *ACS Appl. Mater. Interfaces* **2013**, *5*, 1943−1947.
(34) Wang, Z.; Xu, B.; Zhang, L.; Zhang, J.; Ma, T.; Zhang, J.; Fu, X.; Tian, W. Folic Acid-Functionalized Mesoporous Silica Nanospheres Hybridized with AIE Luminogens for Targeted Cancer Cell Imaging. *Nanoscale* **2013**, *5*, 2065−2072.
(35) Zhang, X.; Zhang, X.; Tao, L.; Chi, Z.; Xu, J.; Wei, Y. Aggregation Induced Emission-Based Fluorescent Nanoparticles: Fabrication Methodologies and Biomedical Applications. *J. Mater. Chem. B* **2014**, *2*, 4398−4414.
(36) Chang, M. C. Y.; Pralle, A.; Isacoff, E. Y.; Chang, C. J. A Selective, Cell-permeable Optical Probe for Hydrogen Peroxide in Living Cells. *J. Am. Chem. Soc.* **2004**, *126*, 15392−15393.
(37) Miller, E. W.; Albers, A. E.; Pralle, A.; Isacoff, E. Y.; Chang, C. J. Boronate-based Fluorescent Probes for Imaging Cellular Hydrogen Peroxide. *J. Am. Chem. Soc.* **2005**, *127*, 16652−16659.
(38) Miller, E. W.; Tulyanthan, O.; Isacoff, E. Y.; Chang, C. J. Molecular Imaging of Hydrogen Peroxide Produced for Cell Signaling. *Nat. Chem. Biol.* **2007**, *3*, 263−267.
(39) Dickinson, B. C.; Huynh, C.; Chang, C. J. A Palette of Fluorescent Probes with Varying Emission Colors for Imaging Hydrogen Peroxide Signaling in Living Cells. *J. Am. Chem. Soc.* **2010**, *132*, 5906−5915.
(40) Rhee, S. G. H_2O_2, A Necessary Evil for Cell Signaling. *Science* **2006**, *312*, 1882−1883.
(41) Finkel, T. Oxidant Signals and Oxidative Stress. *Curr. Opin. Cell Biol.* **2003**, *15*, 247−254.
(42) Park, S.; Yoon, J.; Bae, S.; Park, M.; Kang, C.; Ke, Q. G.; Lee, D. W.; Kang, P. M. Therapeutic Use of H_2O_2-Responsive Anti-oxidant Polymer Nanoparticles for Doxorubicin-Induced Cardiomyopathy. *Biomaterials* **2014**, *35*, 5944−5953.
(43) Yoshii, T.; Onogi, S.; Shigemitsu, H.; Hamachi, I. Chemically Reactive Supramolecular Hydrogel Coupled with a Signal Amplification System for Enhanced Analyte Sensitivity. *J. Am. Chem. Soc.* **2015**, *137*, 3360−3365.
(44) Qiao, J.; Liu, Z.; Tian, Y.; Wu, M.; Niu, Z. W. Multifunctional Self-assembled Polymeric Nanoprobes for FRET-based Ratiometric Detection of Mitochondrial H_2O_2 in Living Cells. *Chem. Commun.* **2015**, *51*, 3641−3644.
(45) Sun, X. L.; Guo, S. J.; Chung, C. S.; Zhu, W. L.; Sun, S. H. A Sensitive H_2O_2 Assay Based on Dumbbell-like PtPd-Fe_3O_4 Nanoparticles. *Adv. Mater.* **2013**, *25*, 132−136.
(46) Luo, Z.; Song, H.; Feng, X.; Run, M.; Cui, H.; Wu, L.; Gao, J.; Wang, Z. Liquid Crystalline Phase Behavior and Sol-Gel Transition in Aqueous Halloysite Nanotube Dispersions. *Langmuir* **2013**, *29*, 12358−12366.
(47) Gai, L. Z.; Mack, J.; Liu, H.; Xu, Z.; Lu, H.; Li, Z. F. A BODIPY Fluorescent Probe with Selective Response for Hypochlorous Acid and Its Application in Cell Imaging. *Sens. Actuators, B* **2013**, *182*, 1−6.
(48) Madejova, J. FTIR Techniques in Clay Mineral Studies. *Vib. Spectrosc.* **2003**, *31*, 1−10.

DOI: 10.1021/acsami.5b08600
ACS Appl. Mater. Interfaces 2015, 7, 23805−23811